Cation Location in Dehydrated Na−Rb−Y Zeolite: An XRD and IR Study

G. L. Marra

ENICHEM S. p. A., Centro Ricerche Novara−"Istituto Guido Donegani", Via G. Fauser 4, I-28100 Novara, Italy

A. N. Fitch

ESRF, BP 220, F-38043 Grenoble Cedex, France

A. Zecchina, G. Ricchiardi, M. Salvalaggio,† S. Bordiga, and C. Lamberti*

Dipartimento di Chimica Inorganica, Chimica Fisica e Chimica dei Materiali, Università di Torino, 10125 Via P. Giuria 7, Torino, Italy

Received: May 30, 1997; In Final Form: September 11, 1997[⊗]

High-quality powder XRD data of a dehydrated Na−Rb−Y zeolite with Si/Al = 2.7, collected at the ESRF beam line BM16, are analyzed. The quality of the Rietveld refinement is very satisfactory, as confirmed by the low R_{wp} and R_p values of 7.77% and 6.02%, respectively, and by the comparison of the Rb^+/Na^+ ratio (1.36(6)) with the experimental one (1.38) obtained by analytical methods. We have found that 9.3(3) Na^+ cations are located in site SI, 8.3(6) Na^+ and 5.4(6) Rb^+ cations in site SI′, and 2.9(6) Na^+ and 22.4(6) Rb^+ cations in site SII. No cations have been observed in site SIII. Less than 4 cations out of 51.8 remain to be located in the unit cell, which has a cell parameter of $a = 24.7673(4)$ Å, ($V = 15192.8(7)$ Å^3). The low occupancy by Na^+ of sites in the supercage (site SII) is confirmed by a parallel IR study of CO and N_2 adsorbed at low temperature, where carbon monoxide and dinitrogen have been found to interact mainly with the Rb^+ cations. The spectroscopic study of the stretching vibrations of $Na^+\cdots CO$ and $Na^+\cdots N_2$ adducts allows the estimation of a Rb^+/Na^+ ratio of approximately 9 in site SII, in close agreement with the ratio obtained from the Rietveld refinement, 8(2).

1. Introduction

Zeolites represent a large family of aluminosilicates constituted by corner-linked TO_4 tetrahedra (T stands for either Si or Al) that adopt a remarkable variety of structures containing channels and/or cavities of different dimensions.[1] The zeolite framework has a net negative charge, arising from AlO_2^- units that replace neutral SiO_2 units, which equals the number of aluminum atoms present in the framework. The electrostatic neutrality is ensured by an equivalent number of extraframework cations. The possible role of the latter as catalytically active sites was already postulated and discussed in the very first papers concerning the catalytic applications of zeolites (see, for example, ref 2). According to these ideas, it has been shown that such ions possess a remarkable polarizing power. In fact, depending on the zeolite structure, the cation charge, radius, and location, extraframework cations expose adsorbed guest molecules to local electric fields on the order of 10^9-10^{10} V m^{-1}.[3−9] These intense fields are supposed to be responsible for the activation and reactivity of adsorbed guests.[9,10] Moreover, the cation and the adjacent negatively charged oxygen atoms provide dual acid−base sites (of the Lewis type) that can also play an important role[11] in many catalytic processes mediated by zeolites.

Since zeolites are easily prepared in different cationic forms, cation exchange provides a means for tuning intrazeolite electric fields. The tunability is even more emphasized when a highly cation-populated zeolite, like Y, is prepared in a bicationic form $A^{n+}-B^{m+}-Y$. In fact, in this case, the occupancy of each site is shared by the two cations, and this adds an additional degree of freedom to the map of intrazeolite electric fields. It is thus evident that an accurate investigation of the local electric fields generated by the cations and the relation to their location is of paramount importance for understanding the catalytic properties of zeolites.

In this work, the complementary use of powder X-ray diffraction (XRD), for the cation location, with infrared (IR) spectroscopy, which is particularly useful for probing the local electric fields, is consequently proposed.

XRD has been used since the earliest times to investigate faujasites[12] (zeolites X and Y), and the locations and occupancies of cations in the different exchanged forms have been reported. Among the studies concerning Na^+ homocationic forms, we mention ref 13−21 and for bicationic Na^+-B^+-Y forms (where B^+ is a monovalent cation) we cite refs 16 and 22−29. Na faujasites have also been studied by powder neutron diffraction.[30−32] Because of the similarity to our study, particular mention must be made of the papers of Shepelev et al. on hydrated Na−Rb−X[28] and of Koller et al.[29] on the powder XRD and ^{23}Na and ^{133}Cs magic-angle spinning (MAS) NMR investigation of Na−Cs−Y.

IR studies of probe molecules adsorbed in channels and cavities have been widely employed to evaluate the strength of local electric fields in microporous solids.[33] In fact, when dosed at low temperature on a dehydrated zeolite, they are adsorbed at cationic sites, and their stretching modes are perturbed by the Stark effect[34] associated with the electric fields generated by the cations and the surrounding environment.[33] The strength of the interaction with the cations depends upon the structure

† Present address: ENICHEM S. p. A., Centro Ricerche Novara−"Istituto Guido Donegani", Via G. Fauser 4, I-28100 Novara, Italy.

* To whom correspondence should be addressed. E-mail: LAMBERTI@TO.INFN.IT. Telephone: +39-11-6707537. Fax: +39-11-6707855.

⊗ Abstract published in *Advance ACS Abstracts,* November 1, 1997.

S1089-5647(97)01747-1 CCC: $14.00

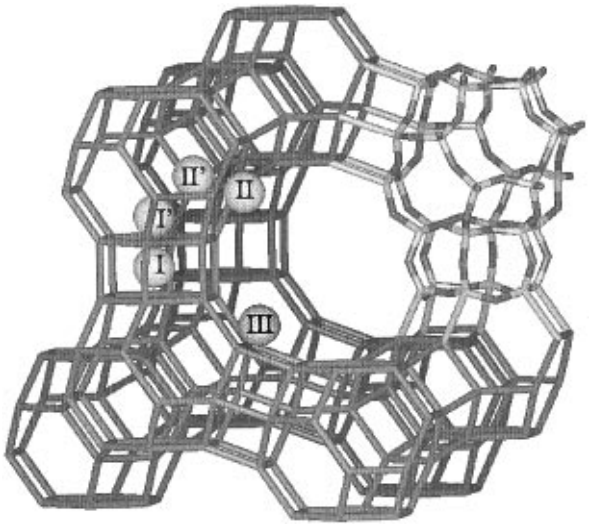

Figure 1. Structure of faujasite, where the location of cation sites SI, SI′, SI**I**, SI**I**′, and SI**II** are shown.

of the molecules used to probe the local electric fields, so the use of molecules with different structures has represented an important means to make IR spectroscopy site and cation sensitive and hence potentially to differentiate between them. Hence, it is becoming an important technique that can complement powder XRD data. Among the different probe molecules used to investigate cation sites in zeolites, the most popular are certainly N_2O,[35] N_2,[36−44] CH_4,[5,45] O_2,[36−38,46] pyridine,[47] CO,[6−8,36−38,48−51] and H_2 (or D_2).[36−38,51−54]

The tridimensional structure of zeolite Y is generated by connecting sodalite units with hexagonal prisms to give a framework characterized by big, empty cavities (supercages) with a diameter of about 13 Å. From the quoted papers, it is recognized that the cations are mainly located in a few well-defined sites (see Figure 1) where the nomenclature of Smith has been adopted.[55] Site SI is located in the center of the hexagonal prism, closely surrounded by six oxygens of the two bases of the prism. Cations located in this site are almost totally inaccessible to guest molecules. This means that they cannot play a direct role in catalytic reactions. Owing to their high coordination, these sites are highly populated. Cations in site SI′ are located on the external basis of the hexagonal prisms just inside the sodalite cage. These cations are surrounded by three oxygens of the basis of the prisms and are accessible only to molecules able to penetrate through a six-membered ring from the supercages into the sodalite cavities. This penetration is not possible even for small molecules such as CO or N_2[49] but occurs for H_2.[51] Owing to Coulombic repulsion, the simultaneous occupation of adjacent SI and SI′ sites is forbidden. Sites SII′ and SII are located in the middle of the six-membered ring forming the frontier between the supercage and the sodalite cage, just inside the sodalite cage and the supercage, respectively. For the same reason mentioned before, adjacent sites cannot be simultaneously occupied. Finally, site SIII is located in the supercage on the two square bases belonging to a sodalite cage and a hexagonal prism, respectively. Such cations have four oxygens as nearest neighbors, which are, however, located at a distance greater than that observed in the other sites. Thus, site SIII shows the highest coordinative unsaturation and is consequently the least occupied. This means that site SII is the most populated site of the supercage and is accessible, together with site SIII, to both CO and N_2 molecules. For the same reason such cations exhibit the highest affinity for molecules and are more easily involved in cation exchange.

TABLE 1: Results of the Elementary Analysis (in atom %)[a]

element	Na−Y	Rb−Y
Si	0.725	0.727
Al	0.275	0.273
Na	0.279	0.109
Rb		0.151

[a] Data have been renormalized by imposing Si + Al = 1. Estimated relative errors are below 5%; see text.

2. Experimental Section

Na−Y, with Si/Al = 2.7, was kindly supplied by Enichem Laboratories Novara (Italy). From this sample, the Rb form was prepared by standard ion-exchange procedures using aqueous solutions of RbCl. Elemental analysis was performed on both samples by measuring the X-ray fluorescence yield of Al, Si, and Na on a Philips PW 1404/10 instrument equipped with a double Sc, Mo anode. The amount of Rb in the exchanged sample was measured with a ICP-MS instrument equipped with a Perkin-Elmer Elan 5000 mass spectrometer. The Na content was also cross-checked by atomic absorption measurements. The results are summarized in Table 1. From these data, we can conclude that an exchange of 58% has been achieved. The confidence level of the compositions reported in Table 1 can be evaluated by considering the differences in Si and Al determination in the two samples and by considering, for each sample, the differences between the Al and the cation content. In all cases the estimated relative error is below 5%.

For IR measurements, thin self-supporting wafers of the zeolite (before and after the cation exchange) were prepared and activated in vacuo at 623 K for 2 h inside an IR cell allowing in situ high-temperature treatments, gas dosage, and low-temperature IR measurements. The IR spectra were recorded in transmission mode, at 2 cm^{-1} resolution, on a Bruker IFS66 spectrometer equipped with a mercury cadmium telluride (MCT) liquid nitrogen-cooled detector. For each sample the spectrum taken at low temperature before dosage of the CO or N_2 gas has been used as background; all the spectra shown in this work are background subtracted. Although the IR cell was permanently cooled with liquid nitrogen, the actual sample temperature was ∼100−110 K.

Powder diffraction patterns were collected on the powder diffraction beam line BM16[56] at the European Synchrotron Radiation Facility (ESRF), Grenoble, France, during experiment CH-107.[57] The beam line was operated with a collimating mirror before the Si(111) water-cooled, double-crystal monochromator, set to deliver a wavelength of $\lambda = 0.84973(1)$ Å, calibrated using the NIST Si standard 640b. λ was chosen to be slightly longer than the wavelength of the Rb K edge (0.816 Å) to minimize the sample absorption. The optional focusing mirror after the monochromator was not used. The sample capillary was spun on the axis of the diffractometer, while the detector bank was scanned from 2 to 60° in 2θ at a rate that varied from 0.5° per minute at low angle to 0.1° per minute at high angle. Data were collected in a continuous scanning mode, with the electronic scalers and the 2θ encoder read around 6 times per second. The total data acquisition lasted a little over 8 h, with the high-angle regions being scanned more than once to improve the statistical quality of the pattern.

The detector bank consists of nine scintillator counters, each behind a separate Ge(111) analyzer crystal, with the nine crystals mounted on a single rotation stage. The separation between each channel is close to 2°. Consequently, nine diffraction patterns, offset one from the other by around 2°, are measured simultaneously. The 2θ angle of the central channel is taken as the nominal 2θ value of the diffractometer arm. Following

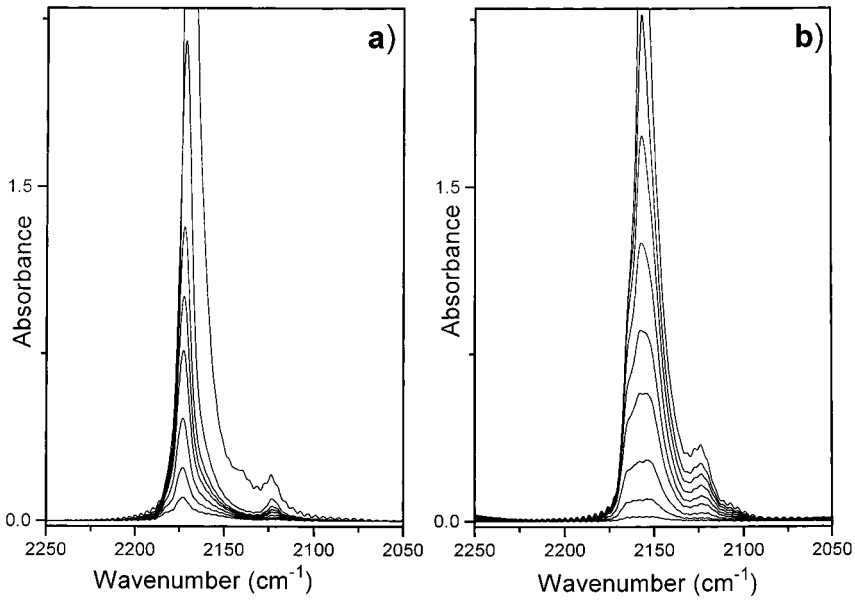

Figure 2. IR spectra of CO dosed, at ∼110 K, at increasing equilibrium pressures from 0.05 to 10 Torr (1 Torr ≈ 133.3 Pa) on Na−Y and Na−Rb−Y in parts a and b, respectively.

data collection, the counts from the nine channels collected at the various positions during the scan are rebinned, taking account of the exact separation between the channels, the different detector efficiencies, and the decrease in the beam current during the scan, to produce the equivalent normalized step scan, which is more suitable for analysis by standard programs. Rejection of the harmonics, $\lambda/3$, $\lambda/4$, etc., that are transmitted by the monochromator and the analyzer crystals is achieved by setting the electronic windows on the detector electronics so that they accept only counts from the fundamental λ.

For the XRD measurements, zeolite powder, activated under dynamic vacuum at 623 K for 2 h, was transferred (in vacuo) into a borosilicate glass capillary 1 mm in diameter. The capillary was sealed, then mounted on the sample spinner on the axis of the diffractometer, which maximizes the number of crystallite orientations presented to the incoming radiation and minimizes the effect of any preferred orientation in the sample.

3. Results and Discussion

3.1. IR Study. In the present study, carried out at ∼110 K, the interaction of CO and N_2 molecules with the Na−Y and with exchanged Na−Rb−Y samples has been investigated, using transmission FTIR spectroscopy, to identify the local electric field and the location of exchanged Rb^+ cations.

Figure 2a reports the IR spectra with increasing CO doses on Na−Y (increasing equilibrium pressures). From this figure it can be clearly seen that only one cation-specific CO band, at 2172 cm^{-1}, is present. This is not surprising, since, unlike H_2,[51,52,54] the larger diameter of the CO molecule (∼3.5−4.2 Å) does not allow it to penetrate into the sodalite cages or hexagonal prisms. Thus, only cations in the supercage (sites SII and SIII) have been probed with this experiment. Since only one cation-specific CO band is observed, we conclude that sites SIII are not occupied in this sample, in agreement with the known fact that they begin to be populated only in zeolites characterized by a lower Si/Al ratio (such as X zeolites).

As far as the minor band at about 2123 cm^{-1} is concerned (Figure 2a), its assignment is for the moment unclear; some authors suggest that it is due to $X^+\cdots OC$ adducts, others that it is due to the fraction of ^{13}C naturally present in the dosed CO, and yet others that it is due to CO molecules simultaneously interacting, through both ends, with two cations. A more detailed discussion of this band has already been given elsewhere.[49,51] However, since this band is of no importance for the purposes of this work, it will not be discussed further.

For the Rb-exchanged zeolite, the relevant spectra collected under the same experimental conditions are reported in Figure 2b. At high coverages, the spectra are dominated by only one cation−CO specific band at a frequency, 2157 cm^{-1}, definitely lower than that illustrated in Figure 2a. For a comparison with the high coverage spectra of Na−Y and Na−Rb−Y, see Figure 3a.

Since it is well-known that the interaction of the dipolar CO molecule (via the carbon end) with centers having a net positive charge shifts the C−O stretching frequency from that of the free molecule (2143 cm^{-1}) to higher values,[58] and that the magnitude of this hypsochromic shift is linearly correlated with the corresponding field strength,[4,6−8,34] and since the interaction of CO with alkali-metal cations in zeolites has been demonstrated to be essentially of an electrostatic nature,[6−8,59] the decrease of the hypsochromic shift, from $\Delta\tilde{\nu} = +29$ cm^{-1} (Na−Y) to +17 cm^{-1} (Rb−Y), allows one to ascribe unambiguously the 2157 cm^{-1} band to $Rb^+\cdots CO$ adducts in the supercage. By use of the E vs $\tilde{\nu}_{C-O}$ relationship of Pacchioni et al.,[34] a local electric field of strength of 5.10 and 2.39 V nm^{-1} is calculated for Na^+ (homoionic sample) and Rb^+, respectively (see Table 2). At low CO coverages, the spectra show clearly a second component at higher frequency due to a small fraction of unexchanged Na^+ cations still present in the supercage. It should be noted that the band ascribed to CO interacting with the residual Na^+ ions is observed at a frequency definitely lower (∼6 cm^{-1}) than that of the $Na^+\cdots CO$ adducts in the homoionic zeolite. This fact is not surprising, since, by moving from Na−Y to Na−Rb−Y, a Na^+ cation located in site SII will observe the replacement of sodium cations located in sites SII of the same supercage by rubidium cations. Since the ionic radii of the two cations are distinctly different ($R_{Na^+} = 0.99$ Å and $R_{Rb^+} = 1.52$ Å [60]), this implies that the two situations are not electrostatically equivalent because the $Na^+\cdots Rb^+$ distances between sites SII in the supercage are considerably lower than the corresponding $Na^+\cdots Na^+$ distances. Note that the Rietveld refinement locates sites Na SII and Rb SII 1.46(1) Å apart (see section 3.2). In conclusion the residual Na^+ ions in the

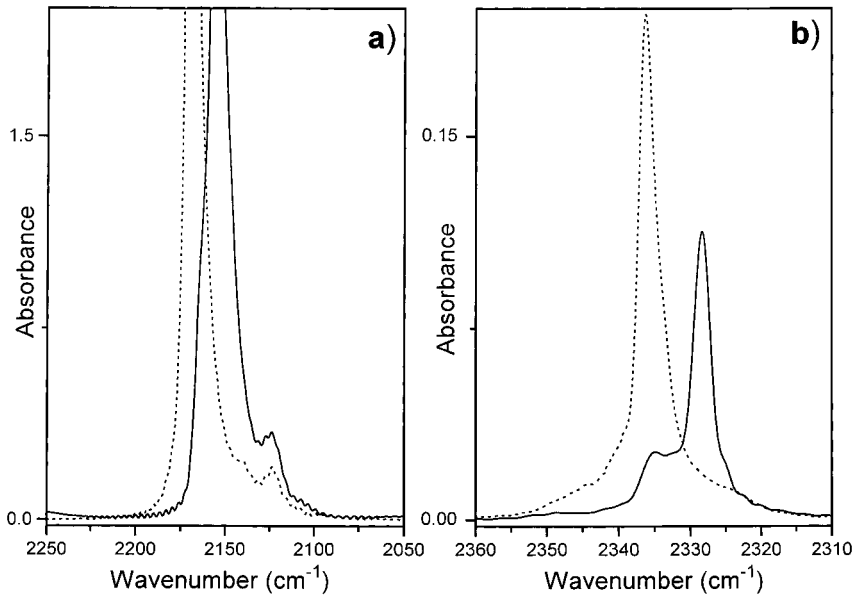

Figure 3. (a) IR spectra of CO (high coverages) dosed at ~110 K on Na−Y and Na−Rb−Y, dotted and full-line curve, respectively. (b) As in part a for N_2 (equilibrium pressures 10 Torr).

TABLE 2: IR Stretching Frequency of the $X^+\cdots CO$ and $X^+\cdots N_2$ ($X^+ = Na^+$ and Rb^+) Adducts in Homoionic Na−Y and in Biionic Na−Rb−Y Zeolites ($\tilde{\nu}_{C-O}$ and $\tilde{\nu}_{N-N}$), Local Electric Field *E* Tested by the Probe Molecule and Computed from the Experimental $\tilde{\nu}_{C-O}$ As Described in Ref 6[a]

zeolite type	$\tilde{\nu}_{C-O}$ (cm^{-1})	$\tilde{\nu}_{N-N}$ (cm^{-1})	*E* (V nm^{-1})
Na−Y	2172, this work and refs 49, 51	2336, this work	5.10
Na−Rb−Y: Na site	2166, this work	2335, this work	4.01
Na−Rb−Y: Rb site	2157, this work	2328, this work	2.39
Na−mordenite	2177, refs 6, 8, 51	2334, ref 43	6.07
Rb−mordenite	2159, refs 6, 8	2328, ref 43	2.74
Na−ZSM-5	2178, refs 6, 7, 49, 51	2334, ref 42	6.26
Rb−ZSM-5	2162, refs 6, 7	2328, ref 42	3.28

[a] The same data concerning ZSM-5 and mordenite, taken from refs 6−8, 42, 43, 49, 51, are reported for sake of comparison.

supercage of sample Na−Rb−Y undergo a consistent radial approach to the other positive charges with a subsequent decrease (from 5.10 to 4.01 V nm^{-1}) of the total electric field as probed by CO adsorbed on them (which is, to a first approximation, the vectorial sum of the local electric field at the Na^+ site and the average contribution of the other cations in the same cage). The same effect has been observed when N_2 has been dosed on both Na−Y and Na−Rb−Y zeolites (vide infra). This explanation is, of course, only qualitative; however, quantitative computation is still in progress.[61]

Note that Förster et al.[38] have already observed that the hypsochromic shift of CO adsorbed on sodium sites in A zeolites moves from $\Delta\tilde{\nu}_{C-O} = +22$ cm^{-1} in homoionic Na−A to $\Delta\tilde{\nu}_{C-O} = (+25) - (+28)$ cm^{-1} in $Na_{12-2x}-Ca_x$ -A as a function of *x*. This is clear evidence that, in highly ion-populated zeolites (such as A, X, and Y), the substitution of the cations surrounding a given adsorption site is a reliable means for tuning the local electric field strength. This collective effect has not been observed in low cation-populated zeolites such as ZSM-5, where the CO stretching frequency of the $Na^+\cdots CO$ adduct has always been observed at 2178 cm^{-1} in Na−ZSM-5, $Li_{0.25}-Na_{0.75}$-ZSM-5, $Rb_{0.9}-Na_{0.1}$-ZSM-5, and $Cs_{0.9}-Na_{0.1}$-ZSM-5 [7] and where the interaction of CO with the adsorption site can be modeled using a local approach.[6]

For the data reported in Figure 2, it is unfortunately impossible to determine in a quantitative way the Rb^+/Na^+ ratio in the supercage, since the formation of $Na^+\cdots CO$ and $Rb^+\cdots CO$ adducts is thermodynamically strongly favored in different pressure ranges and comparison between the spectra reported in parts a and b of Figure 2 is consequently troublesome. From Figure 3a it is evident that the two cation-specific CO bands have a very similar shape and a similar width. This indicates that Rb^+ cations have substituted a high proportion of the Na^+ cations in site SII. At such high coverages, the contribution of $Na^+\cdots CO$ adducts to the spectrum of CO dosed on the Na−Rb−Y sample is represented by a negligible, scarcely visible shoulder. It is therefore impossible to quantify such small amounts of unexchanged sodium cations in the supercage, since both bands reported in Figure 3a are so intense that an evaluation of the optical density at the maximum is not feasible. The IR study of the adsorption of N_2 can allow us to resolve this problem.

To illustrate this, let us mention that the N_2 probe is very interesting, since its homonuclear character implies that the unperturbed molecule has a null dipole moment (the N−N stretching mode is thus Raman but not IR active). However, when N_2 is subjected to an external electric field, like that exerted by a cationic site, it becomes polarized. As a consequence, relaxation of the selection rules occurs with subsequent activation of the IR activity of the stretching vibration. An important advantage of such a molecular probe, compared to CO, is that not only the frequency but also the integrated intensity of the ν_{N-N} band of the $X^+\cdots N-N$ adduct ($I_{X^+\cdots N-N}$) depends dramatically upon the strength of the local electric field *E* generated by cation X^+. In particular Cohen de Lara et al. have found $I_{X^+\cdots N-N}$ to depend on E^2.[40,44] This means that the study by IR spectroscopy of adsorbed N_2 takes advantage not only of the change of stretching frequency induced by the polarizing field but also of the change of the specific intensity. This allows one easily to detect very small amounts of species adsorbed on a lowly populated site with a high polarizing power, even in the presence of a high concentration of a similar adduct on other cationic sites. This is clearly our case because Na^+ cations in site SII, although having a very low site occupancy factor, have a higher polarizing power (with respect to Rb^+). From literature data on ZSM-5 [42] and Mordenites,[43] it is known that $Na^+\cdots N_2$ and $Rb^+\cdots N_2$ adducts give two well-resolved IR bands at 2334 and 2328 cm^{-1}, respectively (see also Table 2).

We can thus use N_2 to probe quantitatively the number of Na^+ ions occupying site SII in Na−Rb−Y.

Figure 3b reports the IR spectra collected at ∼110 K (equilibrium pressure ≈ 10 Torr) of N_2 dosed on Na−Y and Na−Rb−Y samples (dotted and full line spectra, respectively). The dotted spectrum shows only one cation-specific band at 2336 cm^{-1} attributed to the $Na^+\cdots N-N$ complex in site SII, in agreement with the data reported in refs 42 and 43. A second feature of the spectrum is represented by the presence, on both sides of the $Na^+\cdots N-N$ band, of two weak rotovibrational wings (R and P), indicating that N_2 is in a hindered rotational state.[43] The same experiment performed on Na−Rb−Y (full line spectrum) exhibits a major absorption at 2328 and a minor one at 2335 cm^{-1}. We thus attribute the former to $Rb^+\cdots N-N$ adducts and the latter to $Na^+\cdots N-N$, both in site SII. As already observed when CO was dosed, $\tilde{\nu}_{N-N}$ of the $Na^+\cdots N-N$ adduct suffers a reduction of its hypsochromic shift by moving from Na−Y (2336 cm^{-1}) to Na−Rb−Y (2335 cm^{-1}). Because of the smaller global shift of the N_2 molecule compared to CO, when perturbed by the same electric field, the experimental detection of the reduction of the blue shift is in this case borderline, but still meaningful, since it is supported by the parallel unambiguous observation obtained with CO.

An important point needing further discussion concerns the comparison of the N−N stretching frequencies of $Na^+\cdots N-N$ and $Rb^+\cdots N-N$ adducts in Y zeolite and that of dinitrogen in the gas phase ($\tilde{\nu}^{\circ}_{N-N} = 2330$ cm^{-1}). The experimental evidence that N_2 shows a $\tilde{\nu}_{N-N} > 2330$ cm^{-1} when interacting with Li^+ and Na^+ cations (hypsochromic shift) but a $\tilde{\nu}_{N-N} < 2330$ cm^{-1} when interacting with K^+, Rb^+, and Cs^+ (bathochromic shift) has already been reported by Yamazaki et al.[42] and by us[43] for alkali-metal-exchanged ZSM-5 and mordenites, respectively. The two papers give different explanations of this observation. Yamazaki et al.[42] have concluded that, in the small channel of the MFI structure (∼5.5 Å in diameter), the N_2 molecule does not have enough space to form a linear adduct with the larger cations (K^+, Rb^+, and Cs^+) and that the corresponding $X^+\cdots N_2$ adducts must assume a tilted position. The $N_2\cdots X^+$ interaction is consequently not maximized, resulting in a bathochromic effect on $\tilde{\nu}_{N-N}$.

Based on the experimental fact that when CO is dosed on alkali-metal-exchanged ZSM-5 and mordenites, a bathochromic shift of $\tilde{\nu}_{C-O}$ is never observed,[6−8] and with the dimensions of CO and N_2 molecules being very close, we have formulated in ref 43 (section 3.5) the hypothesis that $\tilde{\nu}^{\circ}_{N-N} = 2330$ cm^{-1} is not the correct reference frequency for a dinitrogen molecule adsorbed into the zeolite cavities. In our opinion, a better reference is represented by N_2 perturbed by dispersion forces only (due to the framework acting like a solvent). The reference value should be similar to that of liquid-like dinitrogen or dinitrogen entrapped in cryogenic matrixes. Unfortunately, liquid-like N_2 is IR inactive and we cannot measure it directly;[62] we can just try to estimate $\tilde{\nu}^{\circ}_{N-N}$ by looking at the Raman frequency of N_2 in rare gas matrixes (Ar, 2326 cm^{-1}; Kr, 2324 cm^{-1}; Xe, 2322 cm^{-1})[64] or in silicalite (2324 cm^{-1})[65]. When this is properly done, it transpires that the $\tilde{\nu}_{N-N}$ shift is always hypsochromic, in full agreement with what is observed with CO.[6−8] The data presented here, showing the $\tilde{\nu}_{N-N}$ stretching frequency of the $Rb^+\cdots N_2$ adducts in Y zeolites (where no steric hindrance could be invoked) is still <2330 cm^{-1}, rule out the hypothesis of Yamazaki et al.[42]

For the data presented here, the relatively low intensity of the $Rb^+\cdots N-N$ specific band (full line spectrum) with respect to that of $Na^+\cdots N-N$ (dotted line spectrum) is evident and is due to the decreased IR absorption coefficient of the N−N stretching frequency when the polarizing power of the center decreases (vide supra). Program ASYMGRAD,[66,67] which uses the minimization capabilities of MINUIT,[68] has been used to perform a band fitting of both curves reported in Figure 3b. As a result, we find that $I_{Na^+\cdots N-N}$ (band at 2335 cm^{-1}) is reduced by a factor of 10 in the exchanged form. We thus conclude that site SII is populated by both Rb^+ and Na^+ and that the Rb^+/Na^+ ratio is ∼9. Owing to the uncertainty in the band separation procedure, the precision of this estimate is about 20%.[69]

By combining the results of the elemental analysis and IR spectroscopy of dosed CO and N_2, we are thus able to conclude that Rb^+ cations have substituted nearly all Na^+ ions of site SII and that the remaining Na^+ cations must be located in sites SI, SI′, or SII′ (where they could partially share the occupancy with Rb^+ cations). This picture will be confirmed and quantified by XRD analysis.

3.2. Powder XRD Structure Refinement. The Rietveld refinement[70] has been performed using the software package GSAS (General Structure Analysis System),[71] and a preliminary report has been presented at the EPDIC-5 conference.[72] All technical details adopted for the structure refinement are described in the Appendix. The refinement of the framework atoms in space group $Fd\bar{3}m$ has been done while imposing restraints on the T(Si/Al)−O and O−O distances. As a starting structure, we have used that of Na−Y.[17] The refinement has been performed in three sequential steps. During the first we simply tried to refine the structure starting from the framework atoms without cations. After this step, the difference Fourier map shows three major peaks located in positions very close to those normally reported for sites SI, SI′, and SII, respectively. In the second step, cations were introduced into the model. Since we know from the elemental analysis that sodium is still present, as a first approximation we decided to locate sodium in site SI and rubidium in sites SI′ and SII because cations in site SI are more difficult to exchange and because of the IR evidence that only a very small number of Na^+ ions are present in the supercage. The difference Fourier map then shows two minor peaks located at distances of about 1.5 Å from the refined positions of Rb^+ cations in sites SI′ and SII, indicating that we are dealing in both cases with a site splitting. No appreciable feature was observed in site SI. We have interpreted this fact by assuming that no observable amount of Rb^+ has penetrated the hexagonal prism and that Na^+ is still present in both sodalite and supercage cavities. This hypothesis was in agreement with the fact that the Rb^+/Na^+ ratio obtained from the refinement at this stage was considerably higher than that obtained from the elemental analysis. In the last step we have thus performed the refinement after adding Na^+ ions in sites SI′ and SII, using as starting coordinates those of the corresponding peaks in the difference Fourier map of the previous step. The results of this final refinement are reported in Table 3.

It is worth emphasising that, when referring to rubidium and sodium in site SI′, although using the same label, we are considering two significantly different positions in the structure, since they are separated by 1.64(1) Å in the refinement (which is performed down to *d* spacing smaller than 0.8 Å). The same holds for Rb^+ and Na^+ in site SII, where the two cation positions are separated by 1.46(1) Å. Let us recall that a considerable difference between point charges located in sites Na SII and Rb SII has also been indirectly observed by IR spectroscopy as the electric field probed by CO adsorbed on sodium ions is reduced from 5.10 to 4.01 V nm^{-1} by moving from Na−Y to Na−Rb−Y (see Table 2).

As far as site SIII is concerned, it has not been considered in

TABLE 3: Atomic Parameters Resulting from the Rietveld Refinement[a]

atom	*x*	*y*	*z*	U_{iso} (Å^2)	occupancy factor	site	number of atoms per unit cell
Si	0.1247(2)	−0.0537(2)	0.0356(2)	0.011(1)	0.73	192i	140.16
Al	0.1247(2)	−0.0537(2)	0.0356(2)	0.011(1)	0.27	192i	51.84
O1	0.1067(2)	$\bar{x}$	0	0.023(1)	1	96h	96
O2	−0.0015(3)	*x*	0.1408(2)	0.026(1)	1	96g	96
O3	0.1767(2)	*x*	−0.0357(3)	0.015(1)	1	96g	96
O4	0.1789(3)	*x*	0.3204(4)	0.025(2)	1	96g	96
NaSI	0	0	0	0.089(9)	0.58(2)	16d	9.3(3)
NaSI′	0.0455(3)	*x*	*x*	0.031(4)	0.26(2)	32e	8.3(6)
RbSI′	0.0838(3)	*x*	*x*	0.031(4)	0.17(2)	32e	5.4(6)
NaSII	0.2217(4)	*x*	*x*	0.058(2)	0.09(2)	32e	2.9(6)
RbSII	0.2557(2)	*x*	*x*	0.058(2)	0.70(2)	32e	22.4(6)

[a] Values of R_{wp} and R_p parameters are 7.77% and 6.02%, respectively, and $\chi^2 = 0.8667$. The refined cell parameter is $a = 24.7673(4)$ Å ($V = 15192.8(7)$ Å^3).

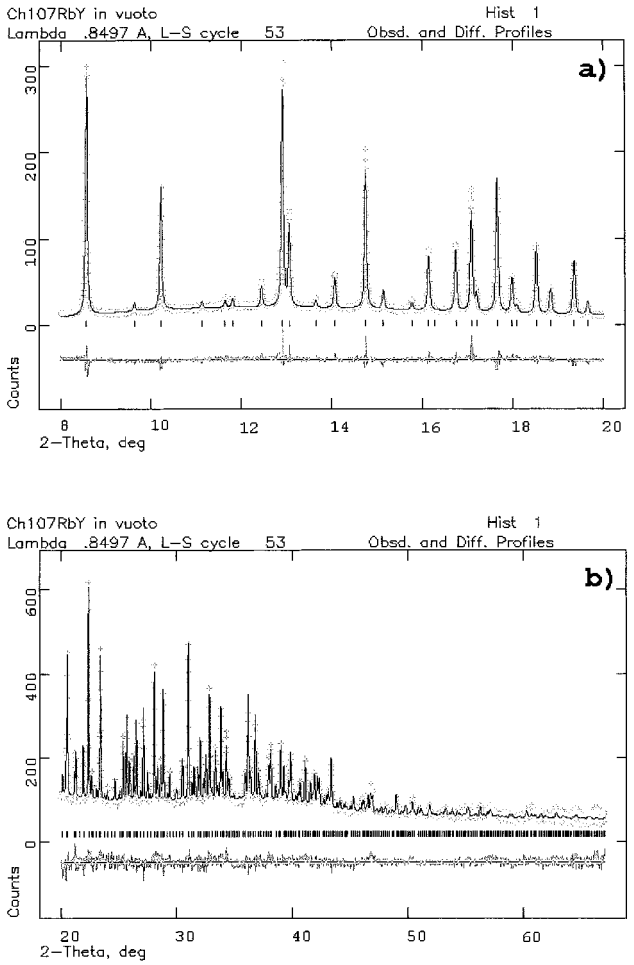

Figure 4. Observed, calculated and difference profiles and reflection positions in low and high 2θ regions in parts a and b, respectively. Ordinate of part a must be multiplied by factor 10.

the refinement because it is usually very scarcely populated in Y zeolites, and there is no evidence of cations being located in it from the IR data (vide supra). The validity of this choice has been fully confirmed by the absence of any features at or near SIII in the difference Fourier map throughout the refinement.

Figure 4 shows the observed and calculated patterns, their difference, and the positions of the diffraction peaks. The quality of the Rietveld refinement is confirmed by the low R_{wp} and R_p parameters (7.77% and 6.02%, respectively). The refined cell parameter is $a = 24.7673(4)$ Å ($V = 15192.8(7)$ Å^3). Our analysis locates 9.3(3) Na^+ cations in site SI, 8.3(6) Na^+ and 5.4(6) Rb^+ cations in site SI′, and 2.9(6) Na^+ and 22.4(6) Rb^+ cations in site SII (see Table 3).

The total occupation of site SI′ is close to the maximum possible, given the occupancy of site SI with 9.3(3) ions per unit cell. Each occupied SI site prohibits occupancy of the two adjacent SI′ sites, because of their proximity (see Figure 1). Hence, the maximum number of occupied SI′ sites is 32 minus twice the number of occupied SI sites, i.e., 13.4(6), which corresponds closely to the sum of the Na SI′ and Rb SI′ sites (13.7(8)). The absence of any relevant amount of charge in site SII′ can be understood by considering that its competitive site (SII) is highly populated with 25.3(8) Na^+ and Rb^+ cations per unit cell).

The absence of any significant peaks of the difference Fourier map (all are below 0.5 electron charge) indicates that no additional cations can be reasonably located in the unit cell. Consequently, no other attempt has been made to improve the refinement.

The high quality of this refinement can also be appreciated by considering the agreement found between the refined parameters and the corresponding values obtained by independent measurements (IR and elemental analysis). The agreement between the Rb/Na experimental ratio (1.38) and the refined one (1.36) is remarkable; the difference between these two values is less than 5% and is compatible with the uncertainty of the data coming from the elemental analysis (see Table 1). Moreover, the refined total number of counterions per unit cell (48(1)) is in very good agreement with the experimental one obtained from the elemental analysis (51.8), since less than four cations remain to be located in the unit cell. Finally, the low population of Na^+ cations in the supercage (only 2.9(6) cations in site SII) is confirmed by the IR study of CO and N_2 adsorbed at low temperature, where carbon monoxide and dinitrogen have been found to interact mainly with the predominant Rb^+ cations. In particular, the spectroscopic study of the interaction of dinitrogen with the remaining Na^+ ions has allowed us to estimate $Rb^+/Na^+ \approx 9$ in site SII, in good agreement with the ratio obtained from the Rietveld refinement (8(2)). It is not surprising that, in this particular case, IR spectroscopy has proved to be more sensitive than XRD for cation location because the main signal contributing to the XRD pattern of the Na−Rb−Y sample comes from the more abundant and more strongly scattering rubidium cations, whereas IR spectroscopy of adsorbed N_2 is much more sensitive to Na^+ rather than to Rb^+ cations, owing to the higher polarizing power of Na^+. The IR investigation is thus of fundamental importance, since it provides a clear starting condition for the Rietveld refinement, very close to the final one.

Because of the similarities to the Na−Rb−Y system, let us finally emphasize that the cation population detailed in our refinement is in general agreement with the recent result published by Koller et al.[29] who have studied with ^{23}Na and ^{133}Cs MAS NMR the Na^+-Cs^+-Y system (Si/Al = 2.49) as a

function of increasing Cs exchange and who have reported the Rietveld refinement from the powder XRD data collected on the 72% cesium-exchanged sample. They found that, with increasing Cs^+ content, the Na^+ cations in sites SII and SI′ are exchanged first and that Na^+ cations in site SI start to be replaced by Cs^+ only at the highest cesium exchange levels.

4. Conclusions

In this work we have presented the parallel and complementary use of synchrotron radiation powder XRD with low-temperature IR spectroscopy to characterize both the cation distribution and the local electric field strengths of a 58% exchanged Na−Rb−Y zeolite with Si/Al = 2.7. IR spectroscopy of adsorbed CO indicates that (i) no cation is present in site SIII, (ii) the amount of sodium present in the supercage is much smaller than that calculated only on the basis of the average Rb/Na ratio obtained from elemental analysis, (iii) the local electric field strength on Rb^+ cation is 2.39 V nm^{-1}, which is a value much smaller than that observed on Na^+ cations in the Na−Y sample (5.10 V nm^{-1}), (iv) the substitution of Na^+ with Rb^+ strongly influences the $\tilde{\nu}_{C-O}$ of carbon monoxide adsorbed on unexchanged Na SII sites, implying that (from an electrostatic point of view) Na^+ and Rb^+ can be considered as point charges located at significantly different positions. The ad hoc choice of a homonuclear IR inactive molecule such as N_2 as probe makes IR spectroscopy extremely sensitive for the evaluation of very small amounts of sodium ions in the supercage and for the measurement of the Rb^+/Na^+ ratio in site SII (∼9). The IR result is of crucial importance, since it provides a starting condition for the Rietveld refinement very close to the final one. The use of synchrotron radiation (beam line BM16 at the ESRF) for XRD has allowed the choice of the optimal wavelength for the Na−Rb−Y zeolite (just longer than that of the Rb−K edge) and the collection of a very high-quality experimental XRD pattern. This has allowed us to perform an accurate refinement able (i) to locate nearly all cations in the unit cell (only less than 4 out of 51.8 are missing), (ii) to reproduce the Rb^+/Na^+ ratio (both average and in site SII) compared with results obtained with independent techniques, and (iii) to quantify the splitting of sites SI′ and SII. Only with such high-quality data has it been possible to localize 2.9(6) Na^+ cations very close to 22.4(6) Rb^+ in site SII.

Acknowledgment. Support from the CNR (*Progetto Finalizzato Chimica Fine II*) and from MURST (40%) is gratefully acknowledged. The authors are indebted to Dr. F. Geobaldo for the cation exchange, to Dr. G. Vaughan for helpful assistance during powder XRD at ESRF and subsequent sophisticated data rebinning, and to L. Meda and L. Grande for the elemental analysis. C.L, G.R., and M.S. thank the ESRF for the financial support during experiment **CH-107**.[57] C.L. thanks C. Otero Areán for fruitful discussions.

6. Appendix: Details of the Structure Refinement

The structure refinement has been performed by the Rietveld method using the software package GSAS (general structure analysis system).[71] The profile function chosen employs a multiterm Simpson's rule integration of the pseudo-Voigt function with up to 17 refinable parameters. This function gives good results fitting asymmetric profiles and shows no correlation with the lattice parameters. In the calculation of structure factors we have taken into account the anomalous dispersion data f' and f'' for each atom calculated for $\lambda = 0.849$ Å by the method of Cromer and Libermann, using the program FPRIME as part of the GSAS suite.[71] During the refinements, the coordinates of oxygens and Si/Al centers have also been optimized, while the occupancies have been kept constant at 1 for oxygens and at 0.73 and 0.27 for Si and Al, respectively, corresponding to the experimental Si/Al ratio of 2.7. The refinement of the framework atoms in space group $Fd\bar{3}m$ has been done imposing restraints on the Si/Al−O and O−O distances in the primary building units.

The isotropic temperature factors are expressed as U_{iso} where the thermal correction to the structure factor is proportional to $\exp[8\pi^2 U_{iso} \sin^2\theta/\lambda^2]$. To reduce the number of fitted parameters, we have used the same isotropic Debye−Waller factor for adjacent sodium and rubidium atoms (i.e., for Na SI′ and Rb SI′ and for Na SII and Rb SII). This means that for those sites, reported U_{iso} values have only an average value. By use of this approach, all elements of the correlation matrix are below 0.75. The structural refinement of Rb−Na−Y has been performed over the angular 2θ range 8°−67°[73] (corresponding to 0.77 Å < d < 6.09 Å) yielding the structural parameters reported in Table 3. The low angular part of the data have been omitted from the minimization cycles, since the background of that part of the spectrum could not be reasonably modeled using the available GSAS background functions.

As far as the adopted minimization routine is concerned, GSAS minimizes the quantity

$$M = \sum_{i=1}^{N} \omega_i [y_i(\text{obs}) - y_i(\text{calc})]^2$$

where i runs over the N points sampled in the chosen angular range, where y_i(obs) and y_i(calc) are the observed and the calculated diffraction intensities for ith point, and where ω_i is the statistical weight associated with the ith point and defined as

$$\omega_i = 1/y_i(\text{obs})$$

The reported weighted and unweighted profile R factors are defined as follows:

$$R_{wp} = [M/\sum_{i=1}^{N} \omega_i y_i^2(\text{obs})]^{1/2}$$

and

$$R_p = \sum_{i=1}^{N} |y_i(\text{obs}) - y_i(\text{calc})| / \sum_{i=1}^{N} y_i(\text{obs})$$

The reported reduced χ^2 value is defined as $\chi^2 = M/(N - n_{var})$, n_{var} being the number of independent parameters refined in the minimization.

References and Notes

(1) Szostak, R. M. *Molecular Sieves*; Van Nostrand Reinhold: New York, 1989. Meier, W. M.; Olson, D. H.; Baerlocher, Ch. *Atlas of Zeolite Structure Types*; Elsevier: London, 1996.

(2) Rabo, J. A.; Angell, C. L.; Kasai, P. H.; Shoemaker, V. *Discuss. Faraday Soc.* **1966**, *41*, 328. Barrer, R. M.; Gibbons, R. M. *Trans. Faraday Soc.* **1965**, *61*, 948. Haynes, H. W. *Catal. Rev. Sci. Eng.* **1978**, *17*, 273. Rabo, J. A. *Catal. Rev. Sci. Eng.* **1981**, *23*, 293, and references therein.

(3) Dempsey, E. *J. Phys. Chem.* **1969**, *73*, 3660. Preuss, E.; Linden G.; Peuckert, M. *J. Phys. Chem.* **1985**, *89*, 2955.

(4) Böse, H.; Förster H.; Schumann, M. In *Proceedings of the 6th International Zeolite Conference*, Reno 1983; Olson D., Bisio, A., Eds.; Butterworths: Guildford, 1984; p 201. Böse H.; Förster, H. *J. Mol. Struct.* **1990**, *218*, 393.

(5) Yamazaki, T.; Watanuki, I.; Ozawa, S.; Ogino, Y. *Langmuir* **1988**, *4*, 433.

(6) Lamberti, C.; Bordiga, S.; Geobaldo, F.; Zecchina, A.; Otero Areán, C. *J. Chem. Phys.* **1995**, *103*, 3158.
(7) Zecchina, A.; Bordiga, S.; Lamberti, C.; Spoto, G.; Carnelli, L.; Otero Areán, C. *J. Phys. Chem.* **1994**, *98*, 9577.
(8) Bordiga, S.; Lamberti, C.; Geobaldo, F.; Zecchina, A.; Turnes Palomino, G.; Otero Areán, C. *Langmuir* **1995**, *11*, 527.
(9) Uytterhoeven, J. B.; Dompas, D.; Mortier, W. J. *J. Chem. Soc., Faraday Trans.* **1992**, *88*, 2753.
(10) Mirodatos, C.; Biloul, A.; Barthomeuf, D. *J. Chem. Soc., Chem. Commun.* **1987**, 149.
(11) Kaeding, W. W.; Butter, S. A. *J. Catal.* **1980**, *61*, 155. Mole, T. *J. Catal.* **1983**, *94*, 423.
(12) Mortier, W. J. *Compilation of extraframework sites in zeolites*; Butterworth: London, 1981, and references therein.
(13) Broussard, L.; Shoemaker, D. P. *J. Am. Chem. Soc.* **1960**, *82*, 1041.
(14) Olson, D. H. *J. Phys. Chem.* **1970**, *74*, 2758.
(15) Eulemberger, G. R.; Shoemaker, D. P.; Keil, J. G. *J. Phys. Chem.* **1967**, *71*, 1812.
(16) Aldrige, L. P.; Pope, C. G. *J. Inorg. Nucl. Chem.* **1974**, *36*, 2097.
(17) Gallezot, P.; Beaumont, R.; Barthomeuf, D. *J. Phys. Chem.* **1974**, *74*, 1550.
(18) Costenoble, M. L.; Mortier, W. J.; Uytterhoeven, J. B. *J. Chem. Soc., Faraday Trans. 1* **1976**, *72*, 130.
(19) Marti, J.; Soria, J.; Cano, F. S. *J. Colloid Interface Sci.* **1977**, *40*, 82.
(20) Rubio, J. A.; Soria, J.; Cano, F. S. *J. Colloid Interface Sci.* **1980**, *73*, 312.
(21) Olson, D. H. *Zeolites* **1995**, *15*, 440.
(22) Maher, P. *Adv. Chem. Ser.* **1971**, *101*, 266.
(23) Mortier, W. J.; Bosmans, H. J. *J. Phys. Chem.* **1971**, *75*, 3327. Mortier, W. J.; Bosmans, H. J.; Uhytteerhoeven, J. B. *J. Phys. Chem.* **1972**, *76*, 650.
(24) Costenoble, M. L.; Maes, A. *J. Chem. Soc., Faraday Trans. 1* **1978**, *74*, 131.
(25) Gellens, L. R.; Mortier, W. J.; Uytterhoeven, J. B. *Zeolites* **1981**, *1*, 11.
(26) Herden, H.; Einicke, W.-D.; Schöllner, R.; Dyer, A. *J. Inorg. Nucl. Chem.* **1981**, *43*, 2533.
(27) Shepelev, Yu. F.; Anderson, A. A.; Smolin, Yu. I. *Zeolites* **1990**, *10*, 61.
(28) Shepelev, Yu. F.; Butikova, I. K.; Smolin, Yu. I. *Zeolites* **1991**, *11*, 287.
(29) Koller, H.; Burger, B.; Schneider, A. M.; Engelhardt, G.; Weitkamp, J. *Microporous Mater.* **1995**, *5*, 219.
(30) Newsam, J. M.; Jacobson, A. J.; Vaughan, D. E. W. *J. Phys. Chem.* **1986**, *90*, 6858.
(31) Fitch, A. N.; Jobic, H.; Renouprez, A. *J. Chem. Soc., Chem. Commun.* **1985**, 284. Fitch, A. N.; Jobic, H.; Renouprez, A. *J. Phys. Chem.* **1986**, *90*, 1311.
(32) Vitale, G.; Mellot, C. F.; Bull, L. M.; Cheetham, A. K. *J. Phys. Chem. B* **1997**, *101*, 4559.
(33) Zecchina, A.; Otero Areán, C. *Chem. Soc. Rev.* **1996**, *25*, 187.
(34) Pacchioni, G.; Cogliandro, G.; Bagus, P. S. *Int. J. Quantum Chem.* **1992**, *42*, 1115.
(35) Cohen De Lara, E.; Vincent-Geisse, J. *J. Phys. Chem.* **1976**, *80*, 1922.
(36) Förster, H.; Schuldt, M. *J. Chem. Phys.* **1977**, *66*, 5237.
(37) Förster, H.; Schuldt, M. *J. Mol. Phys.* **1978**, *47*, 339.
(38) Förster, H.; Frede, H.; Schuldt, M. In *Proceeding of the 5th International Zeolite Conference*, Naples 1980; Rees, L. V. C., Eds.; Heyden: London, 1980; p 458.
(39) Barrachin, B.; Cohen De Lara, E. *J. Chem. Soc., Faraday Trans. 2* **1986**, *82*, 1953.
(40) Cohen De Lara, E.; Delaval, Y. *J. Chem. Soc., Faraday Trans. 2* **1978**, *74*, 790.
(41) Koubi, L.; Blain, M.; Cohen De Lara, E.; Leclercq, J. M. *Chem. Phys. Lett.* **1994**, *217*, 544.
(42) Yamazaki, T.; Watanuki, I.; Ozawa, S.; Ogino, Y. *Bull. Chem. Soc. Jpn.* **1988**, *61*, 1039.
(43) Geobaldo, F.; Lamberti, C.; Ricchiardi, G.; Bordiga, S.; Zecchina, A.; Turnes Palomino, G.; Otero Areán, C. *J. Phys. Chem.* **1995**, *99*, 11167.
(44) Cohen De Lara, E. *Mol. Phys.* **1989**, *66*, 479.
(45) Cohen De Lara, E.; Kahn, R.; Seloudoux, R. *J. Chem. Phys.* **1985**, *83*, 2646.
(46) Jousse, F.; Cohen De Lara, E. *J. Phys. Chem.* **1996**, *100*, 233. Jousse, F.; Larin, A. V.; Cohen De Lara E. *J. Phys. Chem.* **1996**, *100*, 233.
(47) Buzzoni, R.; Bordiga, S.; Ricchiardi, G.; Lamberti, C.; Zecchina, A.; Bellussi, G. *Langmuir* **1996**, *12*, 930.
(48) Bordiga, S.; Escalona Platero, E.; Otero Areán, C.; Lamberti, C.; Zecchina, A. *J. Catal.* **1992**, *137*, 179.
(49) Bordiga, S.; Scarano, D.; Spoto, G.; Zecchina, A.; Lamberti, C.; Otero Areán, C. *Vib. Spectrosc.* **1993**, *5*, 69.
(50) Katoh, M.; Yamazaki, T.; Ozawa, S. *Bull. Chem. Soc. Jpn.* **1994**, *67*, 1246.
(51) Bordiga, S.; Garrone, E.; Lamberti, C.; Zecchina, A.; Otero Areán, C.; Kazansky, V. B.; Kustov, L. M. *J. Chem. Soc., Faraday Trans.* **1994**, *90*, 3367.
(52) Kustov, L. M.; Kazansky, V. B. *J. Chem. Soc., Faraday Trans.* **1991**, *87*, 2675.
(53) Kazansky, V. B.; Borovkov, V. U.; Karge, H. G. *J. Chem. Soc., Faraday Trans.* **1997**, *93*, 1843.
(54) Larin, A. V.; Parbuzin, V. S. *J. Mol. Phys.* **1992**, *77*, 869. Larin, A. V.; Cohen De Lara, E. *J. Mol. Phys.* **1996**, *88*, 1399; *J. Chem. Phys.* **1994**, *101*, 8130.
(55) Smith, J. V. *Adv. Chem. Ser.* **1971**, *101*, 171.
(56) Fitch, A. N. *Mater. Sci. Forum* **1996**, *228*−*232*, 219.
(57) Lamberti, C.; Bordiga, S.; Geobaldo, F. ESRF proposal CH-107, May, 24−26, 1996.
(58) Angell, C. L.; Shaffer, P. C. *J. Phys. Chem.* **1966**, *70*, 1413. Escalona Platero, E.; Scarano, D.; Spoto, G.; Zecchina, A. *Faraday Discuss. Chem. Soc.* **1985**, *80*, 183. Zecchina, A.; Escalona Platero, E.; Otero Areán, C. *J. Catal.* **1987**, *107*, 244. Zecchina, A.; Scarano, D.; Reller, A. *J. Chem. Soc., Faraday Trans.* **1988**, *84*, 2327. Scarano, D.; Spoto, G.; Bordiga, S.; Coluccia, S.; Zecchina, A. *J. Chem. Soc., Faraday Trans.* **1992**, *88*, 291.
(59) Ferrari, A.; Garrone, E.; Ugliengo, P. *J. Chem. Phys.* **1996**, *105*, 4129.
(60) Shannon, R. D. *Acta Crystallogr.* **1976**, *A32*, 751.
(61) Larin, A. V.; Leherte, L.; Vercauteren, D. P.; Lamberti, C.; Bordiga, S.; Zecchina, A. Manuscript in preparation.
(62) Note that the same holds for CO, where molecules adsorbed in the zeolitic cavities, nonspecifically interacting with cations, give rise to an adsorption at 2138 cm^{-1}, i.e., 5 cm^{-1} below that of CO gas.[7,8,48,49,63]
(63) Zecchina, A.; Bordiga, S.; Spoto, G.; Scarano, D.; Petrini, G.; Leofanti, G.; Padovan, M.; Otero Areán, C. *J. Chem. Soc., Faraday Trans.* **1992**, *88*, 2959. Zecchina, A.; Bordiga, S.; Spoto, G.; Marchese, L.; Petrini, G.; Leofanti, G.; Padovan, M. *J. Phys. Chem.* **1992**, *96*, 4991.
(64) Löwen, H. W.; Jodl, H. J.; Lowenschuss, A.; Däufer, H. *Can. J. Phys.* **1988**, *66*, 308.
(65) Saperstein, D. D.; Rein, A. J. *J. Phys. Chem.* **1977**, *81*, 2134.
(66) Lamberti, C.; Bordiga, S.; Cerrato, G.; Morterra, C.; Scarano, D.; Spoto, G.; Zecchina, A. *Comput. Phys. Commun.* **1993**, *74*, 119.
(67) Lamberti, C.; Morterra, C.; Bordiga, S.; Cerrato, G.; Scarano, D. *Vib. Spectrosc.* **1993**, *4*, 273.
(68) James, F.; Roos, M. *Comput. Phys. Commun.* **1975**, *10*, 343.
(69) The error in the deconvolution procedure is mainly due to (i) the presence of lateral rotovibrational tails and (ii) to the small variation of the extinction coefficient of the N−N stretching of $Na^{+}\cdots N-N$ adducts formed in the two cationic forms.
(70) Rietveld, H. M. *Acta Crystallogr.* **1966**, *20*, 508; **1967**, *22*, 151. Rietveld, H. M. *J. Appl. Crystallogr.* **1969**, *2*, 65.
(71) Larson, A. C.; Von Dreele R. B. Report No. LA-UR-68-748; Los Alamos National Laboratory: Los Alamos, NM, 1987.
(72) Fitch, A. N.; Marra, G. L.; Zecchina, A.; Ricchiardi, G.; Salvalaggio, M.; Bordiga, S.; Lamberti, C. Presented at 5th European Powder Diffraction Conference (EPDIC-5), Parma, Italy, May 25−28 1997.
(73) Please note that if the central detector (number 5) is at $2\theta = 60°$, detectors 6, 7, 8 and 9 are at $2\theta = 62°$, 64°, 66°, and 68°, respectively; see Experimental Section.